Response of Mid-Rise Reinforced Concrete Frame Buildings to the 2017 Puebla Earthquake

Carlos A. Arteta,[a)] M.EERI, Julian Carrillo,[b)] M.EERI, Jorge Archbold,[a),c)] M.EERI, Daniel Gaspar,[c)] Cesar Pajaro,[a)] Gustavo Araujo,[a)] Andres Torregroza,[a)] Ricardo Bonett,[d)] Carlos Blandon,[e)] Luciano R. Fernandez-Sola,[f)] M.EERI, Juan F. Correal,[g)] and Khalid M. Mosalam,[c),h)] M.EERI

The response of mid-rise reinforced concrete (RC) buildings in Mexico City after the 2017 Puebla Earthquake is assessed through combined field and computational investigation. The Mw 7.1 earthquake damaged more than 500 buildings where most of them are classified as mid-rise RC frames with infill walls. A multinational team from Colombia, Mexico, and the United States was rapidly deployed within a week of the occurrence of the event to investigate the structural and nonstructural damage levels of over 60 RC buildings with 2–12 stories. The results of the study confirmed that older mid-rise structures with limited ductility capacity may have been shaken past their capacity. To elucidate the widespread damage in mid-rise RC framed structures, the post-earthquake reconnaissance effort is complemented with inelastic modeling and simulation of several representative RC framing systems with and without masonry infill walls. It was confirmed that the addition of non-isolated masonry infills significantly impacts the ductility capacity and increases the potential for a soft-story mechanism formation in RC frames originally analyzed and designed to be bare systems. [DOI: 10.1193/061218EQS144M]

INTRODUCTION

A moment magnitude (Mw) 7.1 earthquake struck the central region of Mexico on 19 September 2017 at approximately 1:14 PM local time [18:14 UTC; National Autonomous University of Mexico (UNAM) 2017]. Although the epicenter of the event was located at approximately 120 km from Mexico City, severe structural damage, including 40 collapses [Mexican School of Civil Engineers (CICM) 2017], were reported at several locations

[a)] Department of Civil and Environmental Engineering, Universidad del Norte, Barranquilla, Colombia; Email: carteta@uninorte.edu.co (C. A. A)
[b)] Department of Civil Engineering, Universidad Militar Nueva Granada, Bogotá, Colombia
[c)] Department of Civil and Environmental Engineering, University of California, Berkeley, CA 94720-1710
[d)] Department of Civil and Environmental Engineering, Universidad de Medellín, Medellín, Colombia
[e)] Department of Civil and Environmental Engineering, Escuela de Ingeniería de Antioquia, Medellín, Colombia
[f)] Department of Materials, Universidad Autónoma Metropolitana-Azcapotzalco, Mexico City, Mexico
[g)] Department of Civil and Environmental Engineering, Universidad de los Andes, Bogotá, Colombia
[h)] Pacific Earthquake Engineering Research (PEER) Center, University of California, Berkeley, CA 94720-1710

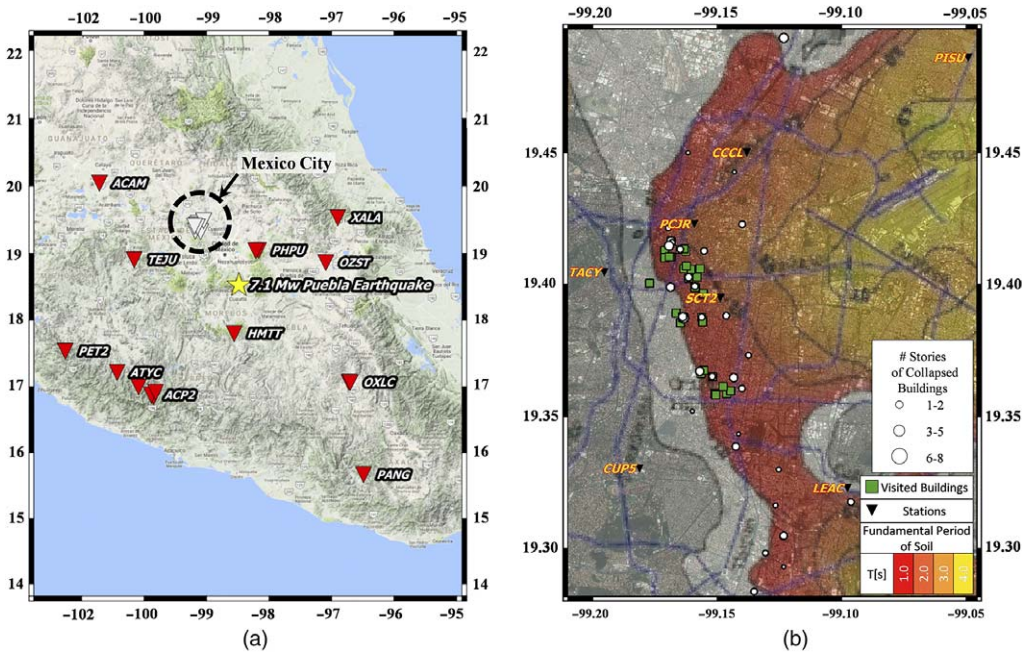

Figure 1. (a) Mw 7.1 Puebla Earthquake epicenter and locations of recording stations. (b) Map of Mexico City with fundamental soil period (NTC-S 2004), showing locations of recording stations and visited buildings.

(Figure 1b). One week after the event, a four-day post-earthquake reconnaissance mission was organized between the Pacific Earthquake Engineering Research (PEER) Center and the Colombian Earthquake Engineering Research (CEER) Network. Once on the ground, the teams joined forces with local researchers, practitioners, and faculty from UNAM and CICM. This joint effort brought together over 20 engineers who conducted a rapid post-earthquake assessment of over 60 buildings (Figure 1b) in the Polanco, Portales Sur, Emperadores, Narvarte, Valle del Centro, and Roma neighborhoods in Mexico City, where the damage was concentrated. Visited sites were located within the "transition zone" as defined by the local Mexico City building code (NTC-S 2004; Figure 1b). This is a zone where the fundamental period of the soil approximately ranges from 1.0 to 2.0 s and is expected to be influenced by basin site effects, as evidenced during previous earthquakes such as the 1985 Michoacán Earthquake (Chávez-García and Bard 1994).

This article studies the response of older mid-rise reinforced concrete (RC) framed buildings to the 2017 Puebla Earthquake. The team verified the seismic performance of the buildings by assessing the response of structural and nonstructural components. Gathered observations and the estimated statistics allowed assembling representative numerical experiments to provide reasonable explanation to the extent of damage observed in mid-rise RC frame buildings with masonry infill walls. These mid-rise buildings were selected in this study, as they are an archetypical engineered and non-engineered structural system in

main cities of Latin American countries and also worldwide. In fact, after masonry structures (55%), RC frame buildings (13%) are the second most common typology in the Andean region [Global Earthquake Model (GEM) 2016]. In addition, most of these RC frame buildings are non–code compliant structures, as they were built several decades ago following outdated design codes or even constructed as non-engineered structures (Reinoso et al. 2016).

GROUND MOTION INTENSITIES

THE MW 7.1 PUEBLA EARTHQUAKE

On September 19, a 7.1 Mw earthquake was recorded at an epicentral distance of 120 km from Mexico City (UNAM 2017). The hypocenter of this event was located right at the edge where the Cocos plate dip-angle increased in its subduction process beneath the North American plate (Mayoral et al. 2017) with epicentral coordinates 18.40 N, 98.72 W and depth of 57 km (UNAM 2017). Figure 1a shows the location of the epicenter and most of the 25 stations that recorded the event. According to the National Earthquake Information Center of the U.S. Geological Survey (USGS 2017), the event corresponded to a normal faulting earthquake with a strike angle of 111° and a dipping angle of 42°. Their finite fault model indicates that the total slip ranged between 0.5 and 3.0 m, concentrated over an area of approximately 225 km^2.

The hypocentral distance from Mexico City was approximately 140 km. As shown in Figure 1a and 1b, the event was recorded at several locations with various site conditions in Mexico. Strong motion acceleration records were provided to the PEER-CEER reconnaissance team by the National Seismological Service at UNAM. Table 1 presents a summary of the horizontal-component ground motion parameters recorded at each of the 25 stations. Following the PEER NGA-West 2 procedure, acceleration records were filtered using an acausal fourth-order Butterworth high-pass filter with cutoff frequencies at 0.01 Hz and 25 Hz (Ancheta et al. 2014). For each station, the summary data include its location as well as the relative distance from the source, using the rupture distance parameter R_{rup} in km (Bommer and Akkar 2012). Regarding intensity- and duration-related data, the summary contains maximum values in two horizontal directions for the PGA, peak ground velocity (PGV), Arias intensity (I_a), significant duration from 5% to 95% of the I_a threshold (D5-95), and the average of the two horizontal directions for the predominant period (T_m).

Among the stations that recorded the earthquake, seven were in Mexico City. The stations are georeferenced and mapped together with the soil microzonation in the Mexico City building code (NTC-S 2004) in Figure 1b. Stations TACY and CUP5 are located on rock, and the others are located in soft soils. The source-to-site distance among the stations in Mexico City [i.e., CCCL (soil), CUP5 (rock), LEAC (soil), PCJR (soil), PISU (soil), SCT2 (soil), and TACY (rock)] did not vary much (e.g., less than 15 km). However, the site and topographic effects are aspects that may explain the variation in the recorded intensity values. As shown in Table 1, minimum and maximum recorded PGA were 0.06 and 0.20 g at the CUP5 and LEAC stations, respectively.

I_a values at stations located in soil sites were larger than those at stations at rock sites. The LEAC station recorded the ground motions with the largest I_a, although there were not as many damaged buildings reported in the surrounding area, in contrast to the PCJR station,

Table 1. Horizontal-component ground motions

Station ID	Latitude	Longitude	R_{rup} (km)	PGA (g)	PGV (cm/s)	Ia	Duration D5-95 (s)	T_m (s)
ACAC	16.85	−99.85	207	0.060	3.6	0.139	63.8	0.41
ACAM	20.04	−100.72	263	0.005	4.9	0.001	100.7	1.48
ACP2	16.87	−99.89	207	0.036	1.3	0.038	53.2	0.25
ATYC	17.21	−100.43	215	0.019	2.0	0.013	53.0	0.22
CCCL[a]	19.45	−99.14	120	0.075	72.6	0.369	60.8	1.06
COYC	17.00	−100.09	208	0.019	3.9	0.011	50.2	0.20
CUP5[a]	19.33	−99.18	111	0.060	9.1	0.127	35.8	0.78
HMTT	17.80	−98.56	70	0.147	11.9	0.319	26.5	0.33
LEAC[a]	19.32	−99.10	108	0.199	27.8	1.242	40.0	0.79
OXBJ	17.07	−96.72	210	0.018	1.8	0.013	36.0	0.40
OXLC	17.07	−97.09	212	0.023	3.1	0.017	39.0	0.54
OZST	18.86	−97.09	141	0.012	2.1	0.006	61.5	0.67
PANG	15.67	−96.49	341	0.005	1.6	0.001	64.2	0.59
PCJR[a]	19.42	−99.16	118	0.101	25.6	0.958	65.6	1.82
PET2	17.54	−101.26	272	0.010	2.1	0.003	54.4	0.28
PHPU	19.04	−98.17	97	0.142	9.0	0.483	25.3	0.42
PISU[a]	19.49	−99.05	120	0.097	28.1	0.638	92.1	1.66
SCT2[a]	19.39	−99.15	116	0.092	20.7	0.538	58.7	1.10
SXPU	19.04	−98.22	96	0.142	17.0	0.478	30.3	0.64
TACY[a]	19.40	−99.20	118	0.064	10.2	0.119	32.9	0.74
TEJU	18.90	−100.16	150	0.085	4.2	0.054	23.1	0.24
UNIO	17.99	−101.81	314	0.006	3.0	0.001	51.4	0.50
URUA	19.42	−102.07	354	0.006	2.6	0.001	69.4	0.86
VNTA	16.91	−99.82	199	0.011	1.6	0.005	56.2	0.33
XALA	19.53	−96.90	192	0.008	12.1	0.005	76.6	0.92

[a] Stations located in Mexico City.

which recorded the second largest I_a value. The CCCL station recorded the largest values of PGV, and the PISU station recorded the largest values of duration, D5-95. The PCJR motion has the largest period T_m, which is explained, in part, by the location of this station on the lake bed, where soil periods are between 1.0 and 2.0 s.

The linear regression in Equation 1 describes the mean PGA scaling with distance. In this case, the geometric mean of the PGA per station is used:

$$\ln PGA = C_0 + C_1 \ln R_{rup} \tag{1}$$

where the intercept $C_0 = 9.14$, the slope $C_1 = -2.46$, and the coefficient of correlation $R = 0.88$. In contrast, the Mw 8.2 Chiapas Earthquake of 7 September 2017, which occurred 12 days before, has a larger intercept of $C_0 = 10.45$ but a similar slope (i.e., attenuation with distance) of $C_1 = -2.37$; the coefficient of correlation for this event is $R = 0.82$. According to this simple regression, the 2017 Chiapas Earthquake, being the second strongest event in

Mexico since 1787, induced ground motions that were, on average, approximately four-times larger than those induced by the 2017 Puebla Earthquake.

The 2004 version of the Mexico City building code (NTC-S 2004) includes two procedures for seismic design of buildings, one listed in the main code document and other in its appendix A. In the main document of NTC-S and in previous versions of the building code, the spectra were not related to the elastic seismic demands because the elastic design spectrum was reduced by dividing the spectral ordinates by a seismic force factor that accounted for ductility, redundancy, and over-strength. On the other hand, the spectra specified in appendix A of NTC-S (2004) are site specific, and values of the over-strength parameter are explicitly specified (Carrillo et al. 2014). This appendix A of NTC-S (2004) considers three main seismic zones: Zone I (hard soil deposits) with fundamental periods lower than 0.5 s, Zone II (transition zone with layers of clay, silt, and even sand) with fundamental periods between 0.5 and 1.0 s, and Zone III (lake bed zone with large clay layers) with fundamental periods between 1.0 and 5.0 s. Zone III is subdivided into four different zones depending on the thickness of the clay deposits (a, b, c, and d). In the 1985 Mexico Earthquake, the damage was concentrated on Zone IIIb, with fundamental periods between 2.0 and 3.0 s. For the 2017 Puebla Earthquake, the damage was concentrated on Zone IIIa, with fundamental periods between 1.0 and 2.0 s. Figure 2 shows the code-based response spectra for each station in Mexico City based on appendix A of NTC-S (2004), with the corresponding ground motion (e.g., geomean of the two horizontal components) recording during the 2017 Puebla Earthquake. It is worth noting that the 2004 design spectra were developed using a return period of 125 years (Ordaz et al. 2003).

According to CICM (2017) and confirmed by the reconnaissance team, most of the severely damaged and collapsed buildings were located at sites where the thickness of the clay deposits was between 15 and 30 m, which concurs with Zone IIIa of the appendix A of NTC-S (2004). Based on Figure 1b, these soils have a fundamental period between 1.0 and 2.0 s. From wave theory (Kramer 1996), it can be demonstrated that the average shear-wave velocity of such soils is between 60 and 120 m/s. Only for stations CCCL and

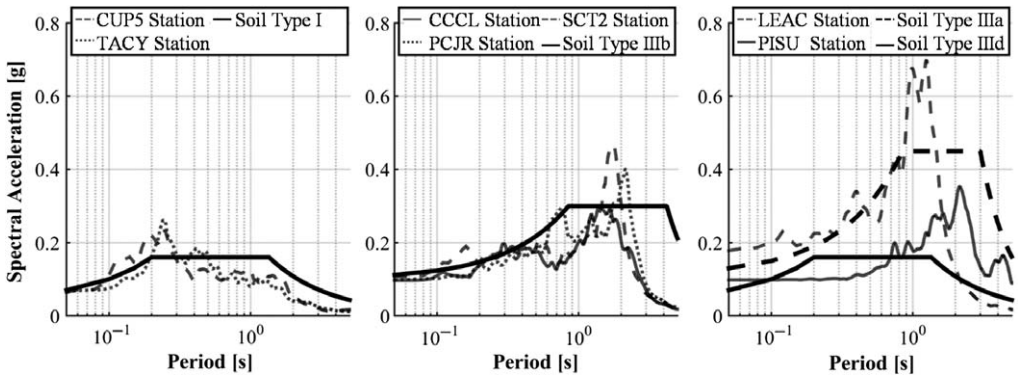

Figure 2. Comparison of code-based design response spectra (appendix A of NTC-S 2004), 5%-damped, and ground motions recorded in Mexico City during the 2017 Puebla Earthquake.

PCJR were the recorded pseudo-spectral acceleration (PSA) values lower than the code-based design spectra at all periods. The PSA values at both the CUP5 and TACY stations were higher than those recommended by the building code for structural periods (T) lower than 0.3 and 0.5 s, respectively. In general, the response spectra recorded in the transition zone peaked between 1.0 and 3.0 s period. The LEAC station recorded PSA values that surpassed the code-based spectral accelerations in the period range 0.9–2.0 s. It is worth mentioning that most of the affected and visited buildings were located around the SCT2 and PCJR stations, where the recorded spectra only surpassed the design code level spectral acceleration over a narrow range of periods close to 2.0 s.

COMPARISON WITH GLOBAL AND LOCAL GROUND MOTION PREDICTION MODELS

The BCHydro ground motion prediction equations (GMPEs) (Abrahamson et al. 2016) were developed as a part of the probabilistic seismic hazard analysis of the hydroelectric company BCHydro at its dams in Canada. It is a global subduction model developed based on a data set of 9,946 ground motion record pairs from 292 subduction zone earthquakes occurring worldwide, such as in Japan, South and Central America, and Mexico, among others. Figure 3 compares PSA values recorded during the Mw 7.1 2017 Puebla Earthquake at the stations in Table 1, with the median ground motion estimate from the BCHydro GMPE. Ground motion estimates from a local GMPE developed by Garcia et al. (2005) are also presented. The comparison is made for PGA and structural periods of 0.5, 1.0, and 2.0 s as a function of R_{rup}. Stations outside Mexico City are depicted as white dots, and those located in Mexico City are depicted with triangular and squared markers representing rock and soil sites, respectively. To account for the different site conditions in Mexico City, the median values of the BCHydro GMPE were estimated using shear-wave velocity at 30 m depth, V_{S30}, of 80 and 760 m/s for soft soils (e.g., the alluvial basin in the city) and rock sites, respectively. The Garcia et al. (2005) GMPE does not differentiate among different soil classes, as it is calibrated for a NEHRP soil type B.

As shown in Figure 3, the median ground motion of the local model follows well the distance versus PSA trend for the stations outside Mexico City. Nevertheless, it underpredicts the recorded ground motions within the city, especially those recorded on soil sites. For $T = 0.5$ s, the PSA values recorded at most soil sites were below the corresponding median BCHydro model, while for $T = 1.0$ s, most of the stations recorded ground motions close to the median BCHydro estimates. For $T = 2.0$ s, recorded PSA values at soil sites are larger than the median estimates of the global model. To quantify how representative the recorded ground motions in Mexico City were, Figure 4 presents the residual between the observed PSA values and the median estimates from the BCHydro model. The results show the bias for each of the seven stations considered in Mexico City for structural periods from 0.5 to 2.5 s, which are representative of the periods of the damaged and collapsed structures. The residuals were estimated as the natural logarithm of the quotient of the observation and the estimation (i.e., residual $= \ln(\mathrm{PSA}_{\mathrm{Observed}}/\mathrm{PSA}_{\mathrm{Estimated}})$, where positive residuals are associated with observations larger than the median model.

In Figure 4, the residuals for the rock sites (CUP5 and TACY) are invariant to structural period. On the other hand, except for the LEAC station, the residual at soil sites (CCCL,

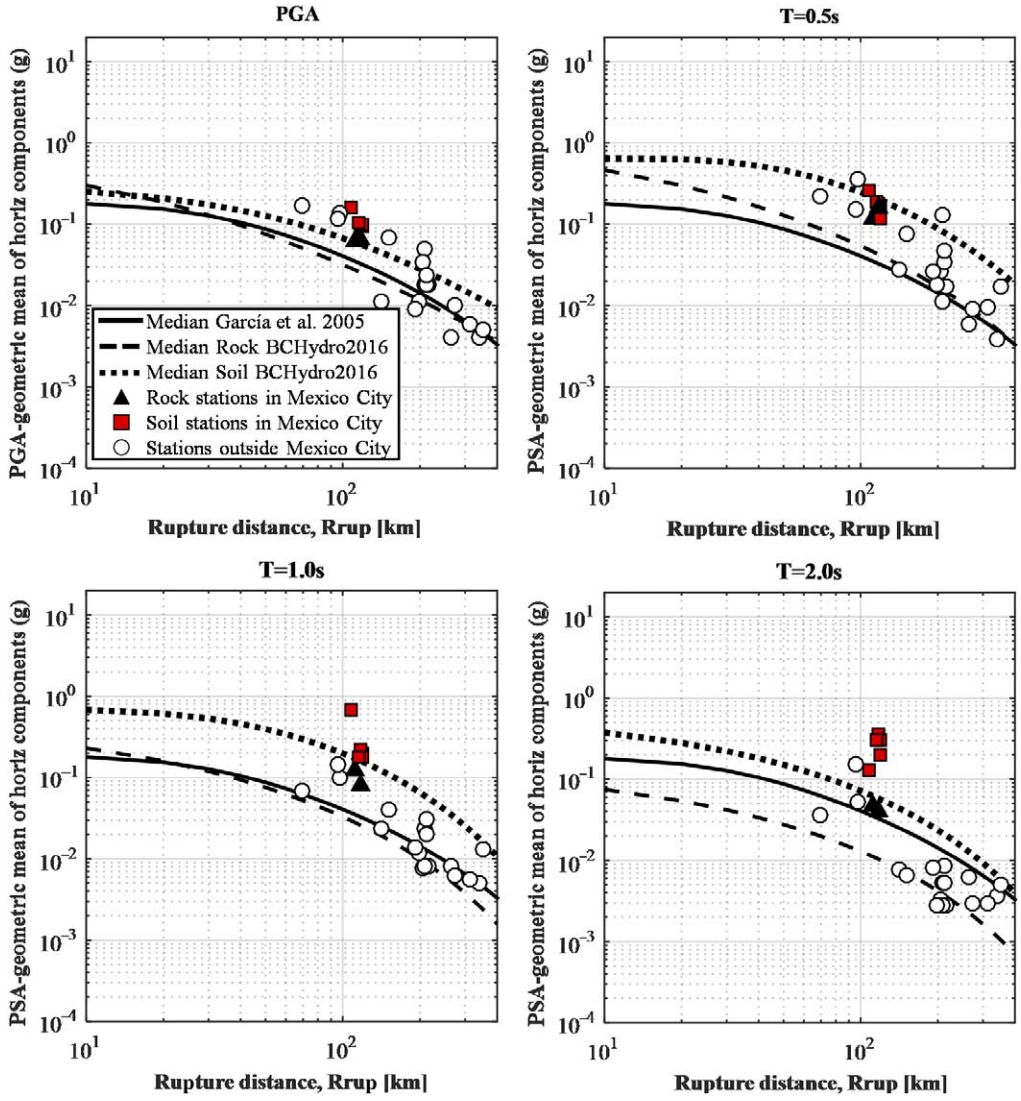

Figure 3. Comparison of recorded pseudo-acceleration data with the BCHydro and Garcia et al. (2005) GMPE predictions.

PCJR, PISU, and SCT2) exhibit a monotonically increasing trend in the range $0.5 \leq T \leq 2.0$, to then flatten or reduce for larger periods. Similar observations are made by Sahakian et al. (2018); ground-motion models underpredict the recorded accelerations at soil sites in Mexico city for periods close to the fundamental period of the deposits because of the basin effects. It is worth emphasizing that for periods larger than 1.0 s, the residual for all stations is positive, with a maximum of 1.75. That is, the recorded ground motions were, in some cases, approximately 5.7-times larger than the median ground motion predicted for the site conditions and

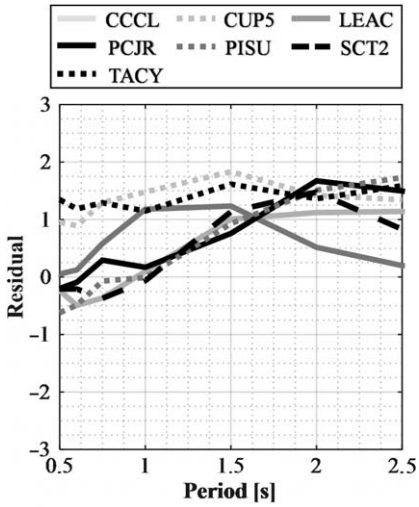

Figure 4. Residuals of Mexico City ground motions between the observed PSA values and the median estimates from the BCHydro model.

distance of a Mw 7.1 earthquake. Among the soil sites, the LEAC station exhibits the largest residuals in the range $0.5 \leq T \leq 1.5$, recording ground motions as large as 3.5-times the median level of the global model. For larger periods, this station exhibits the lowest residual among any station. Stations PCJR and SCT2 are located closer to sites where most damage was observed. For $T = 0.5$ s, the recorded ground motions at these two stations were 1.2-times smaller than the median estimate of the BCHydro GMPE; for $T = 1.0$ s, both stations exhibit residual values close to 0.0, but this trend increases linearly up to $T = 2.0$ s, where these two stations recorded ground motions that are approximately 5-times larger than the median prediction model.

BUILDING CODE EVOLUTION IN MEXICO CITY

Mexico City building code has a long history, and similar to American standards, this history has been shaped by experiences from devastating earthquakes that have unveiled important structural vulnerabilities and technical areas in need of further development. The timeline depicted in Figure 5 summarizes the Mexico City building code development. It is worth mentioning that the RCDF up to its most recent version (2017) does not prohibit nonductile structural design in zones of high seismicity like Mexico City.

STRUCTURAL RECONNAISSANCE

The PEER-CEER team was on site for 4 days giving support to the CICM-UNAM reconnaissance and tagging brigades. As stated before, the epicenter of the earthquake was located approximately 120 km South of Mexico City. Several smaller cities were closer to the epicenter and experienced severe damage because of the earthquake. However, given that the reconnaissance mission was carried out a week after the event, the government advised

1920 [Code Published]
- First version of Mexico City's building Code (RCDF)

1942 [Code Update]
- Buildings classified according to their importance and potential risk to society upon catastrophic failure.
- Seismic Coefficients introduced as constant values dependent only on building classification.

1957 [Earthquake]
- Acapulco earthquake (M_s = 7.9)
- Soft soil amplification effects observed.

1958 [Emergency Adnm]
- Emergency addendum to RCDF
- Seismic coefficients are a function of building classification, building type, soil type and building height.
- ASD allowable stresses increase for elements under seismic loading.
- LRFD method introduced.
- Provisions for torsional oscillations included.

1966 [Code Update]
- Modal dynamic analysis firstly introduced.
- Design spectrum, including structural damping effects included.
- Soil classification is modified. Structure classification by importance is re-arranged. Structure types are redefined.

1976 [Code Update]
- "*Normas Tecnicas Complementarias*" are introduced. These constitute the official guidelines for designing and detailing structural elements of different materials.
- Ductile concrete detailing provisions at plastic hinge locations included. (Optional).
- Included specifications for flat-slabs-supported-by-RC- columns as a lateral force resisting system.
- Static analysis restricted to structures lower than 60 meters in height.
- Seismic force reduction factors accounting for structural system ductility are introduced for the first time. Q factors.
- Weak-story restrictions are included for ductile structural systems.

1985 [Earthquake]
- The Mexico City Earthquake (M_w = 8.0)
- Flat slabs supported by RC columns proved to be a very inefficient lateral force resisting system.

1985 [Emergency Adnm]
- Emergency addendum to RCDF
- Overall increment to seismic coefficients. Especially for long period structures on soft soils.

1987 [Code Update]
- Adopted most emergency addendum provisions into the code.
- Ductile concrete detailing provisions very similar to current ones. (Optional)
- Flat-slabs-supported-by-RC-columns buildings are "penalized" by considerable increments in design forces.
- Structural irregularity conditions are defined. Such as: torsional eccentricity, reentrant corners, large diaphragm openings, soft-stories, etc.
- Q factors are reduced by 20% for irregular structures.

1993 [Code Update]
- Minor updates

2004 [Code Update]
- Detailed zonation of the city based on soft soil characterization.
- Static analysis is prohibited for buildings taller than 20 to 40 meters, depending on irregularity conditions and soil type. As an alternative modal dynamic analysis or response history analysis can be utilized.
- Appendix included for transparent elastic spectrum determination. The transparent elastic spectrum depends on the site's natural period (T_s). The design spectrum can be determined by combining the transparent elastic spectrum with an explicit overstrength factor (R) and the inelastic reduction factor (Q). (Optional)

2017 [Code Update]
- Transparent elastic spectrum appendix becomes part of the code as the prescribed method to determine the design spectrum.
- Non-linear response history analysis becomes mandatory for buildings taller than 80 to 120 meters, depending on irregularity conditions and soil type
- Diaphragm minimum design loads included.
- Amongst many other updates…

Figure 5. Timeline of Mexico City Building Code evolution.

against visiting sites close to the epicenter for safety reasons. Consequently, the PEER-CEER team focused its reconnaissance efforts in Mexico City, where minimum safety standards were met according to the local jurisdiction. The reconnaissance mission was carried out from 27 to 30 September 2017, visiting over 60 sites tagged for apparent damage. The team received logistic help from the CICM and researchers from UNAM to focus the visit on evaluating multistory RC structures. A main task was to determine if any building was under imminent collapse risk. Any knowledge gained on the status of apparently compromised structures was shared to the local authorities, through CICM, to expedite the critical decision-making process. Assembling an international team with graduate students and researchers that natively speak Spanish, with the support from local authorities, researchers, and practitioners on site, proved to be an effective approach to rapidly respond and efficiently assess disaster-affected areas.

STATISTICS OF THE DAMAGED BUILDINGS IN MEXICO CITY

The teams that supported the CICM reconnaissance effort inspected around 2,100 buildings. Approximately 25% of these buildings were identified with some type of structural damage, while 61% were tagged as buildings without structural damage. The remaining 14% of the buildings could not be correctly tagged for different reasons (CICM 2017). Damage associated with the soil-foundation system was observed in 51% of the buildings tagged with structural damage. Figure 6a shows the ratio of nondamaged to damaged buildings for different heights, including the number of visited buildings in each category. The height of about 86% of the buildings inspected varied between 1 and 8 stories. Out of the 933 buildings inspected with 1–3 stories, 26% were marked as damaged. Additionally, a total of 880 buildings with 4–8 stories were visited, out of which 28% were marked as damaged. The statistics of taller buildings show a

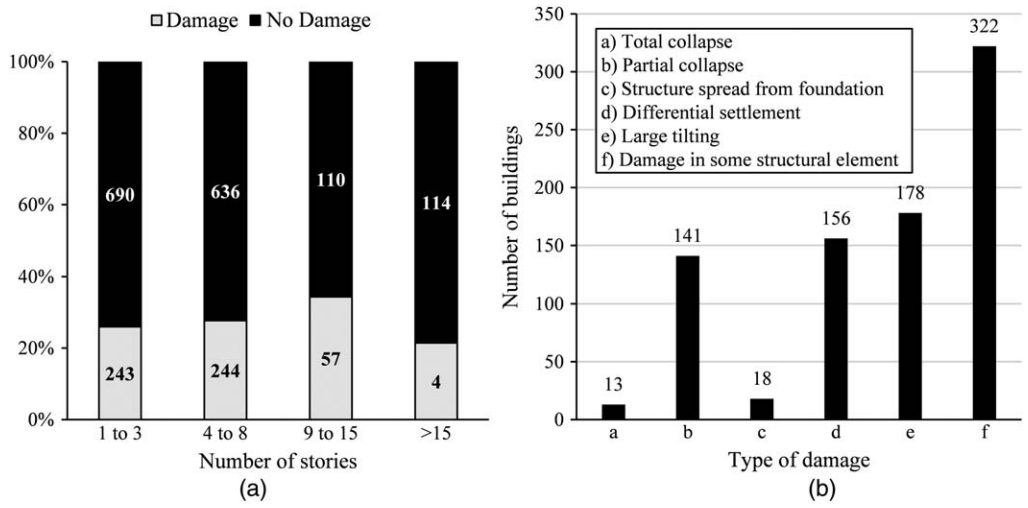

Figure 6. Statistics from the CICM reconnaissance team. (a) Ratio of nondamaged to damaged buildings in terms of their height; (b) number of buildings with different types of damage.

similar trend, although the number of visited structures with more than 9 stories was smaller. Figure 6b shows the distribution of different types of damage. Shown categories are not exclusive; hence a single building may be tagged with various types of damage. More than 150 buildings (i.e., ~7.5% of inspected structures) were catalogued as partially or totally collapsed, while 322 buildings (i.e., 16% of inspected structures) had some type of structural damage. The damage associated with soil-structure interaction, including tilting, was assigned to 352 buildings (i.e., 18% of inspected structures).

Overall, a wide spectrum of performance levels was observed by the PEER-CEER team, from perfectly healthy and undamaged structures to partial or complete collapses. Figure 7 shows examples of damage observed during the reconnaissance mission. The main focus of the visit was assessing frame-type structures, as this typology represents at least 13% of the engineered buildings in urban areas of several Latin American countries (GEM 2014). A significant percentage of these structures were built using outdated design guidelines, namely regulations before the great Mexico City earthquake of 1985, that allowed relatively flexible frames and poor transverse reinforcement detailing and did not provide specific conditions to isolate the nonstructural walls from the main structure. Furthermore, the use of a flat slab supported by RC columns is still allowed, even though it has been widely documented that this type of structure does not perform well during earthquake excitation.

Figure 7. Examples of observed damages: (a) nonstructural damage, (b) structural damage, and (c) collapses.

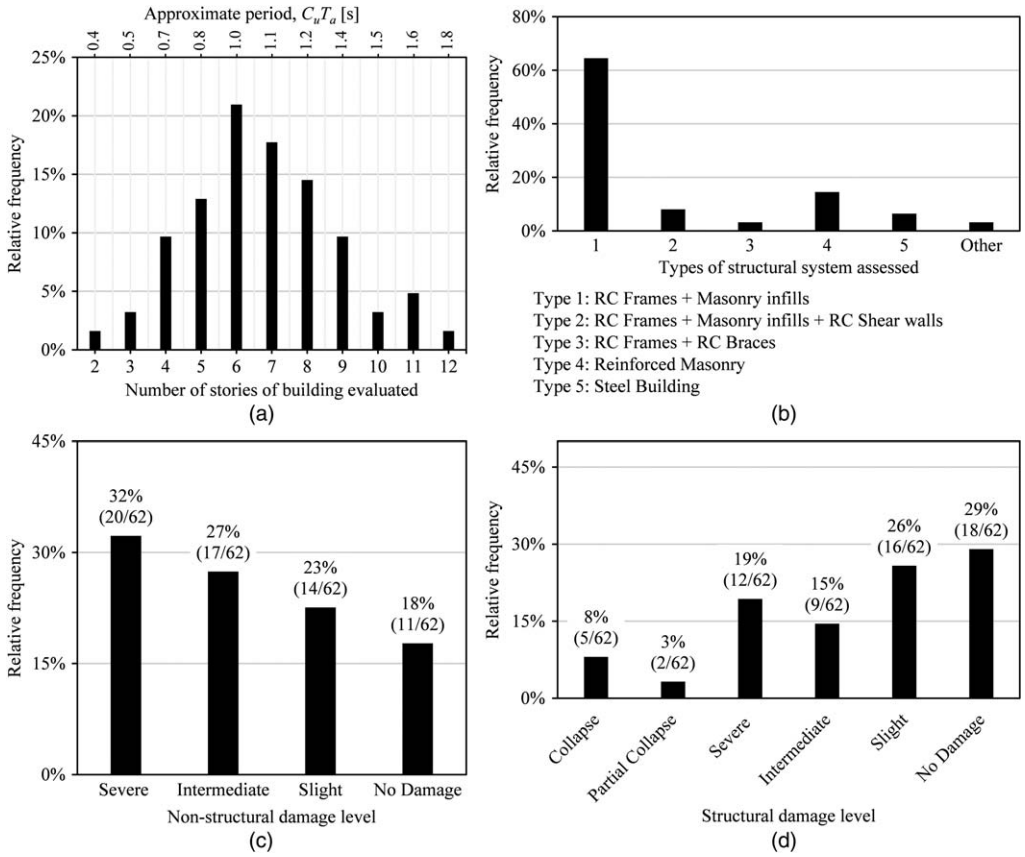

Figure 8. Statistics of inspected buildings by the CEER-PEER team: (a) building height, (b) type of structural system, (c) categories of nonstructural damage, and (d) categories of structural damage.

Additionally, the extensive lack of enforcement of the building codes contributed to the poor performance of some of the structures affected by the earthquake.

Figure 8 summarizes the statistics of the observations made in the field by the PEER-CEER team. A total of 62 buildings were investigated. The buildings had between 2 and 12 stories, with the majority in the range of 5 to 8 stories. The structural period C_uT_a ranged between 0.4 to 1.8 s and was evaluated following *ASCE 7-16* [American Society of Civil Engineers (ASCE) 2016] recommendations (Figure 8a). The approximate fundamental period is $T_a = C_t h_n^x$, where h_n is the structural height in meters, and coefficients $C_t = 0.047$ and $x = 0.9$ are those of concrete moment-resisting frames. Coefficient C_u is taken as 1.4 to lessen the conservatism inherent in the estimation of T_a and to be consistent with structural periods of flexible buildings [*FEMA-P1050-1*; Federal Emergency Management Agency (FEMA) 2015]. Structural periods computed following *ASCE 7-16* (ASCE 2016) recommendations fit in the range of periods measured in instrumented buildings in Mexico (Muriá and González 1995). As shown in Figure 8b, most of these buildings are described as RC frames with masonry infills (over

60% of the cases); other RC framed structures comprised masonry infills with shear walls or RC braces. Buildings with reinforced masonry comprised 15% of the investigated structures, while only four (i.e., ~6.0% of the inspected buildings) steel buildings were investigated.

The type of nonstructural damage was catalogued into the following four categories (Figure 8c): (1) no damage, (2) slight, (3) intermediate, and (4) severe (for examples, refer to Figure 7a). These four categories were adapted and modified from the ones presented by the European Seismological Commission (ESC) in *their European Macroseismic Scale* (ESC 1998). The EMS-98 developed a damage classification of concrete and masonry buildings based on qualitative attributes. The definition of the four nonstructural damage categories can be found in Table 2.

Approximately 60% of the buildings were catalogued as having intermediate or severe nonstructural damage. The investigated RC buildings commonly used masonry as interior and exterior infill walls. According to Meli (1994), the most popular masonry unit in Mexico is a very soft solid clay brick. Furthermore, the Mexican Provision regarding the specifications and test methods for masonry, *NMX-C-404* (ONNCE 2012), states that the thickness of the masonry units commonly used in Mexico ranged from 10 to 14 cm. A common practice is to exclude these walls from being part of the lateral load–resisting systems. Instead, they are only considered in the analytical models as gravitational loads exerted on the beams of the RC frame. However, only in rare occasions are these walls fully separated laterally from the main structural system. Thus once these types of structures are subjected to lateral loads such as earthquakes, the stiff walls attract a major part of the lateral in-plane and out-of-plane loads while they are still intact. Because these walls are typically not properly designed for such effects, they may fail. Many studies in the literature have shown the vulnerability of RC frames with masonry infills (e.g., Mehrabi et al. 1996, Han-Seon and Sung-Woo 2002, Crisafulli et al. 2005, Hashemi and Mosalam 2006, Mosalam and Günay 2015). In general, buildings with widespread nonstructural damage had several masonry infill panels with extensive cracking (catalogued as intermediate damage) and/or partial or total collapse of masonry units, usually on the façade planes. The Mexican construction code does not require

Table 2. Classification of nonstructural damage

Damage level	Definition
No damage	Minimal to no loss of function of the components, it has no impact on the performance of other elements, and building can be used after the seismic event
Slight	Moderate loss of function of the components, no life hazard. Some minor repairments may be needed and some areas of the building will be closed down during repair time
Intermediate	Large and extensive damage of nonstructural components but no life-threatening risk. Functionality of the building will be partly affected and repair work required
Severe	Serious failure of nonstructural components. Severe interruption of the functionality of the building and possibly will carry a high life hazard

separation between adjacent buildings. Hence pounding of structures was also observed in some cases, causing localized major damages of masonry infills, as shown in Figure 7b.

The type of structural damage was catalogued into six categories from no damage to collapse (Figure 8d). An approximately uniform range of damage levels (average of about 22%) from undamaged to severely damaged were observed in buildings. Approximately 30% of the buildings were catalogued as having severe or worse structural damage, including five collapsed buildings. Typically, structures with intermediate damage had visible cracks with no spalling in columns and beams. Severely damaged structures exhibited concrete cover spalling in columns or shear walls, usually near the base of the building or within the lower third of the building height, showing signs of rebar buckling or lap splice failures (see Figure 7b). Other severely damaged columns exhibited signs of incipient development of planes of shear failure.

CASE STUDY: SEISMIC RESPONSE OF 6-STORY BUILDINGS TO THE 2017 PUEBLA EARTHQUAKE

ELASTIC ANALYSIS AND CODE-BASED DESIGN

Although a continuous updating process of the building code in Mexico City is apparent, there are still many pre-1985 flexible nonductile structures that were exposed to the 2017 Puebla Earthquake, some of which were severely damaged. To provide an explanation to the damage observed in older mid-rise buildings, two sets of 6-story RC buildings with moment frames and different configurations of masonry infills (fully or partially infilled) are studied. One set of buildings was designed for low ductility while the other for intermediate ductility, satisfying the NTC-S (1976) and NTC-C (1976) provisions, which were the regulations in force in Mexico from 1976 until 1987. This archetype is considered here because it was one of the most common structural systems with damage reported by the reconnaissance team.

The structural plan of the case-study buildings is shown in Figure 9a. It comprises four 4-bay frames in the EW direction and five 3-bay frames in the NS direction, with span length of 6.0 m. The first story is slightly taller than the other typical stories. The vertical elements of the lateral force–resisting system are connected through a two-way beam-supported slab of 0.10 m in thickness, which is considered as a rigid diaphragm. For design, the concrete compressive strength was defined as $f'_c = 28$ MPa, although it was reduced to $0.80f'_c$ for design purposes, as specified by the Mexican regulations. All reinforcement was assumed Grade 60 ($f_y = 420$ MPa). The elastic modulus was 16,700 MPa for all RC elements, as indicated in the NTC-C (1976).

The 1976 NTC-S prescribed the seismic strength of the structures based on their ductility factor Q, which takes discrete values of 1, 2, 4, and 6 proportionally to their expected deformation capacity. Design seismic forces are estimated by reducing the elastic response spectrum by factor Q'. This seismic-force reduction factor is defined in the code as a function of Q, the structural period (T), and the location within Mexico City. For example, in Zone III of soft soils, $Q' = Q$ for $T > 0.8$ s. Figure 10c shows the 1976 elastic ($Q = 1$) and reduced design spectra for Q values of 2 and 4 for Zone III of soft soils in Mexico City.

Two ductility factors were considered for design; one set of buildings was designed for $Q = 2$ (low ductility) and the other for $Q = 4$ (intermediate ductility). The regulations

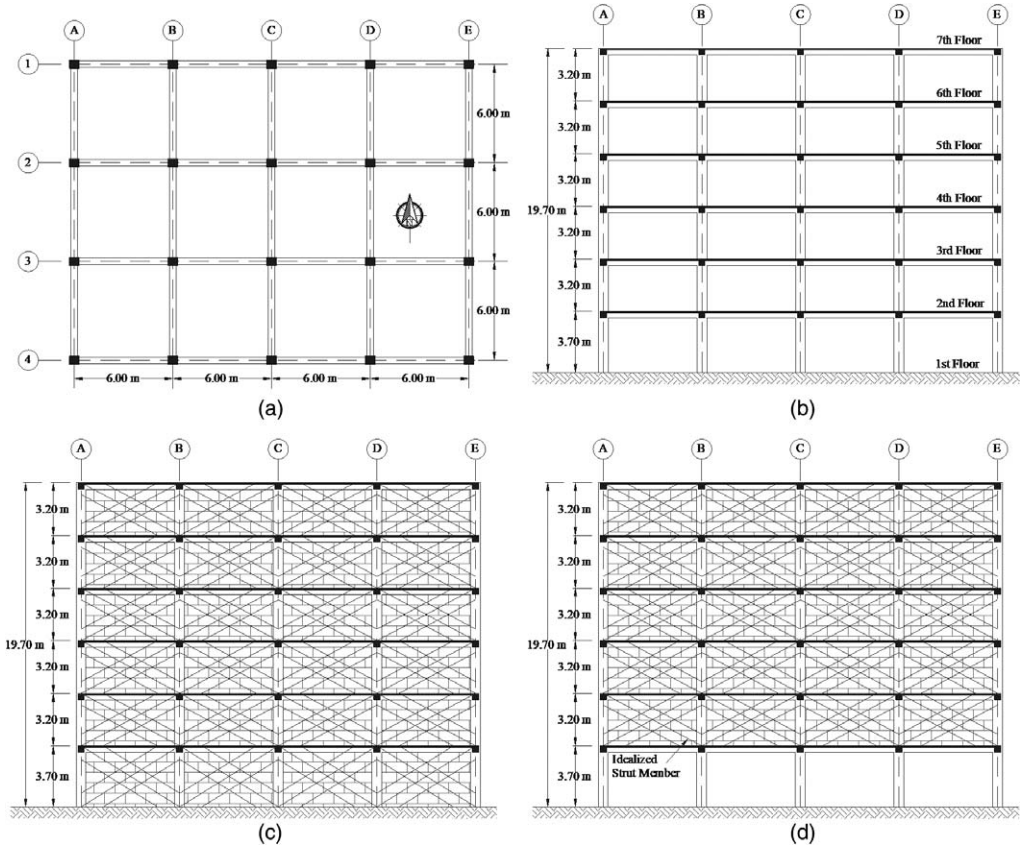

Figure 9. (a) Structural plan of the case-study building. Elevation view of the building, including idealization for lateral nonlinear analysis for the following cases: (b) bare RC frame, (c) fully infilled frame, and (d) partially infilled frame with soft story.

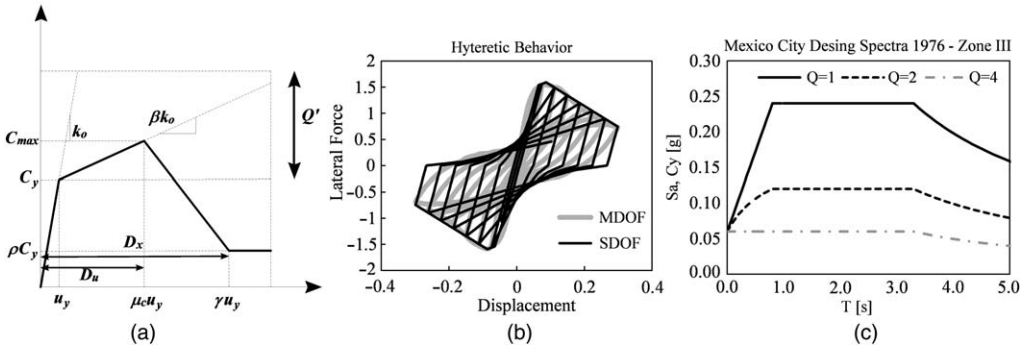

Figure 10. ISDOF model and design spectra: (a) backbone of the ML-model, (b) hysteretic behavior of the ML-model, and (c) 1976 design spectra in terms of *Sa*.

allowed engineers to use either a linear static analysis or a linear dynamic analysis to compute the design seismic forces. For the case-study buildings, a linear static analysis was implemented because of their symmetry and regularity. The elastic model did not account for reduction in stiffness caused by concrete cracking and reinforcement slip from connections or for the existence of infills. The impact of infills on the response is only evaluated in the inelastic domain, as explained below.

The total building weight per unit area for each story, including superimposed dead loads that account for the presence of infills, is $7.7\,\mathrm{kN/m^2}$, with total seismic weight $W = 20{,}000\,\mathrm{kN}$. The seismic base shear, V_S, is estimated as the product of the seismic coefficient, c and W. Values of c range from 0.16 (for rocks and firm soils) to 0.24 (for soft soils). For the case study, a value of $c = 0.24$ was selected because most of the observed collapsed structures were built on soft soils, as categorized in NTC-S (1976). The elastic (uncracked) fundamental vibration periods for design of the bare frame building with $Q = 2$ were 1.46 and 1.35 s for the NS and EW directions, respectively. Those of the weaker building, designed for $Q = 4$, were 1.49 and 1.45 s for the NS and EW directions, respectively. Resulting design base shear for the NS direction, including reduction by Q', are $V_S(Q = 2) = 2{,}484\,\mathrm{kN}$ (i.e., $V_S/W = 12.4\%$) and $V_S(Q = 4) = 1{,}218\,\mathrm{kN}$ (i.e., $V_S/W = 6.1\%$).

Concrete sections were sized and detailed according to the NTC-C (1976). The main difference between the low and intermediate ductility sections was the implementation of the plastic hinge detailing provisions, according to Section 4.7 of the NTC-C (1976), for the building with $Q = 4$. While the NTC-S (1976) only requires this type of detailing for $Q = 6$ (high ductility), it was deemed appropriate herein in the interest of capturing the impact of ductility on the structural response. The $Q = 2$ building was designed as an ordinary moment frame. The reader is referred to Table 3 for the reinforcement detailing of both designs.

INELASTIC MODEL

The expected behavior of the case-study buildings under representative demand from the 2017 Puebla Earthquake was assessed by means of inelastic analyses considering static and dynamic loading effects. The software package Open System for Earthquake Engineering Simulation, OpenSees (McKenna et al. 2000), was selected for this purpose. As shown in Figure 9b–9d, a two-dimensional model representative of the structural framing in the EW direction was selected for nonlinear analyses. As mentioned before, the following three types of variations were implemented in this study to consider different plausible as-built conditions when the earthquake occurred: a bare RC frame (as designed; Figure 9b), a fully infilled RC frame (Figure 9c), and a partially infilled RC frame with a soft story (Figure 9d). A total of six models were studied: two sets of ductility factors each with three variations of the building configuration.

Beams and columns were modeled to include axial and flexural deformations only, using nonlinear elements with distributed plasticity and fiber sections at the integration points (Spacone et al. 1996). Shear was modeled as elastic springs. Second-order P-delta effects were considered in columns. Concrete was modeled as either confined or unconfined, depending on location within the cross section. Linear softening post-peak branch of the concrete model was regularized according to Coleman and Spacone (2001) to

Table 3. Detailing of columns and beams

	Model	ID	Section	Longitudinal reinforcement	Transverse reinforcement
Columns	$Q=2$	1A, 1E, 2A, 2E	60 × 50 cm	First story: $\rho=2.39\%$ Second to fifth story: $\rho=0.53\%$ Sixth story: $\rho=0.75\%$	No. 3 rectangular hoop+rectangular tie at 20 cm for the entire height
		1B, 1C, 1D, 2B, 2C, 2D	60 × 50 cm	First story: $\rho=2.55\%$ Second story: $\rho=0.75\%$ Third to sixth story: $\rho=0.53\%$	No. 3 rectangular hoop+rectangular tie at 20 cm for the entire height
	$Q=4$	1A, 1E, 2A, 2E	50 × 50 cm	First story: $\rho=0.64\%$ Second to fifth story: $\rho=0.52\%$ Sixth story: $\rho=0.64\%$	No. 3 square hoop+square tie at 10 cm near joint at 20 cm elsewhere
		1B, 1C, 1D, 2B, 2C, 2D	50 × 50 cm	First story: $\rho=0.77\%$ Second to sixth story: $\rho=0.52\%$	No. 3 square hoop+square tie at 10 cm near joint at 20 cm elsewhere
Beams	$Q=2$		40 × 40 cm	First to third story: top, $\rho=1.88\%$, bottom, $\rho=0.84\%$ Fourth to sixth story: top, $\rho=1.54\%$, bottom, $\rho=0.58\%$	No. 3 square hoop at 20 cm entire length
	$Q=4$		40 × 40 cm	First to third story: top, $\rho=1.14\%$, bottom, $\rho=0.44\%$ Fourth to sixth story: top, $\rho=0.99\%$, bottom $\rho=0.44\%$	No. 3 square hoop at 10 cm near joint at 20 cm elsewhere

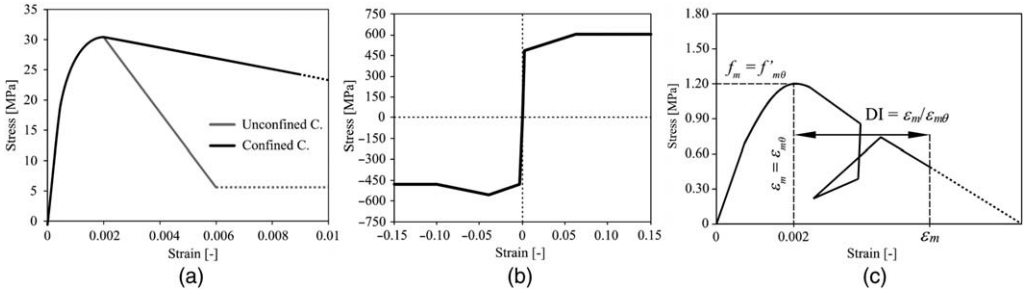

Figure 11. Stress-strain relationship for (a) concrete, (b) reinforcing steel, and (c) masonry struts.

enforce objectivity in the local and global post-peak response (Figure 11a). Fracture energy of concrete in compression (Jansen and Shah 1997) was considered as 25 N/mm and 150 N/mm for unconfined and confined concrete, respectively. Tensile concrete strength was assumed to be $0.62\sqrt{f'_c}$ [MPa], with a strain softening branch adjusted to a fracture energy of 0.1 N/mm (Wittmann et al. 1988). The tensile and compressive behavior of reinforcing steel is asymmetric, as the effects of reduction in compressive strength because of rebar buckling are considered (Arteta 2015). For this purpose, the uniaxial material implemented in OpenSees is the Hysteretic Material. Material parameters to model the cyclic response of the steel were set to simulate a trilinear backbone (Figure 11b) curve with $f_{y+} = 483$ MPa at $\varepsilon_s = 0.0024\,(1.15 f_{y,\text{nominal}})$ using Mazzoni et al. (2007) recommendations.

The hysteretic behavior of masonry infills was modeled using a nonlinear compression-only multi-strut model (Crisafulli 1997, Chrysostomou et al. 2002). The struts are modeled with truss elements whose cross-sectional area and location in the frame depend on the geometrical and mechanical properties of the masonry infills and the RC frame. Masonry wall thickness was assumed to be 0.10 m, and the total equivalent strut width was defined as $0.18 d_m$, where d_m is the length of the masonry wall diagonal. Considering the brick compressive strength as $f'_{cb} = 7.0$ MPa and its tensile strength as $f'_{tb} = 0.9$ MPa, the compressive strength of the strut material is determined according to Crisafulli (1997) as $f'_{m\theta} = 1.2$ MPa. Strain at peak-stress was considered as $\varepsilon_{mo} = 0.002$, while its ultimate stress and strain capacities were taken as $f_{u\theta} = 0.02$ MPa and $\varepsilon_{mu} = 0.010$, respectively (see constitutive relationship scheme in Figure 11c).

NONLINEAR STATIC ANALYSES

Nonlinear static analyses (pushovers) were performed using a lateral load pattern proportional to the fundamental mode shape to investigate the actual strength and the global deformation capacity of the structures. The analyses were terminated when the roof drift ratio reached 2.5% for infilled frames and 3.5% for bare frames, as these displacements ensured modeling a 20% loss of capacity with respect to the peak strength. Pushover curves are shown in Figure 12a. To facilitate the analysis of the inelastic static response, the pushover curves of the frame for the six construction conditions can be approximated to a trilinear model that allows estimating its ductility capacity, μ_c. We use this data in the following

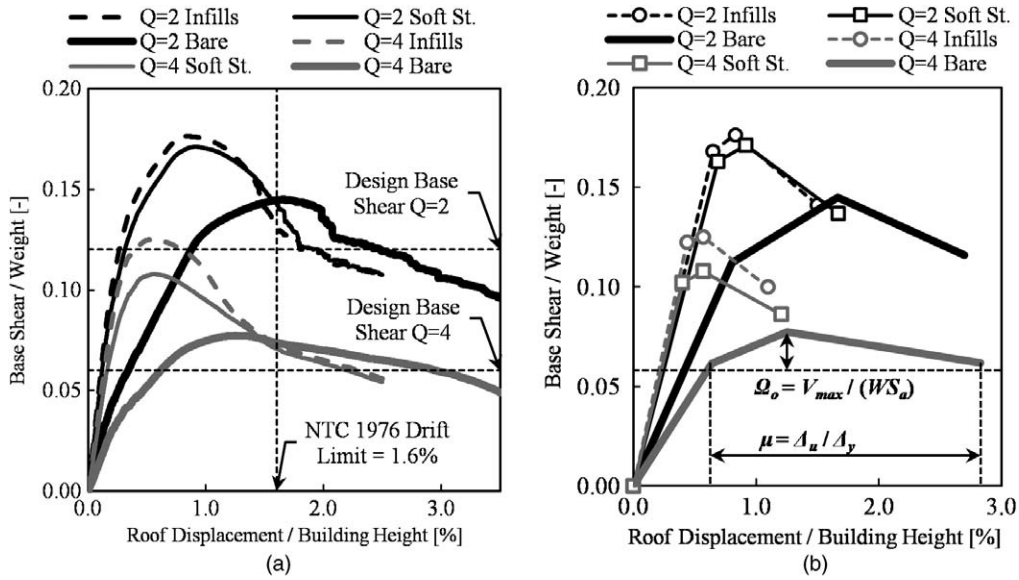

Figure 12. (a) Pushover curves for fully infilled RC frame, RC frame with soft story, and bare RC frame. (b) Trilinear idealization of the pushover responses to determine the ductility capacity.

section to simulate the response of structural systems with similar features to typical Mexican RC frames but in a wider range of periods using inelastic single-degree-of-freedom (ISDOF) models. The trilinear model is bounded by the following three limit states: yielding (Δ_y, V_y), maximum base shear (Δ_{max}, V_{max}), and ultimate capacity (Δ_u, V_u). Yield capacity is selected in this study as the instant in which the first plastic hinge in the structure is formed (i.e., yield curvature ϕ_y is exceeded). Ultimate capacity is selected as the instant in which capacity drops in the post-peak range to 80% (i.e., $V_u = 0.8V_{max}$). The procedure to estimate the yield and ultimate displacements of the structures is consistent with *FEMA-P695* (2009). Figure 12b presents the trilinear idealized model for the six conditions evaluated.

Figure 13a shows the roof drift associated with the three limit states previously defined. A main observation from the pushover analyses is that infills increase strength by 30% on average while decreasing the deformation capacity by at least 38%. Figure 13b shows that there is not a proportional relationship between the actual ductility capacity μ and the code-based ductility factor Q, as the NTC 1976 provisions intended, especially when masonry infills are considered as part of the lateral force–resisting system. While the bare frame designed for $Q = 2$ and 4 had ductility capacities of approximately 3.5 and 4.5, respectively, those of the buildings with masonry had reduced ductility capacity of about 2.5 for $Q = 2$ and between 2.5 and 3.0 for $Q = 4$. For the bare frames, Figure 13c suggests an overstrength factor of 1.2 and 1.3 for the designs with $Q = 2$ and 4, respectively. If the masonry infill is considered, actual overstrength factor for the as-built conditions are at least 1.4 and 1.8 for the designs with $Q = 2$ and 4, respectively.

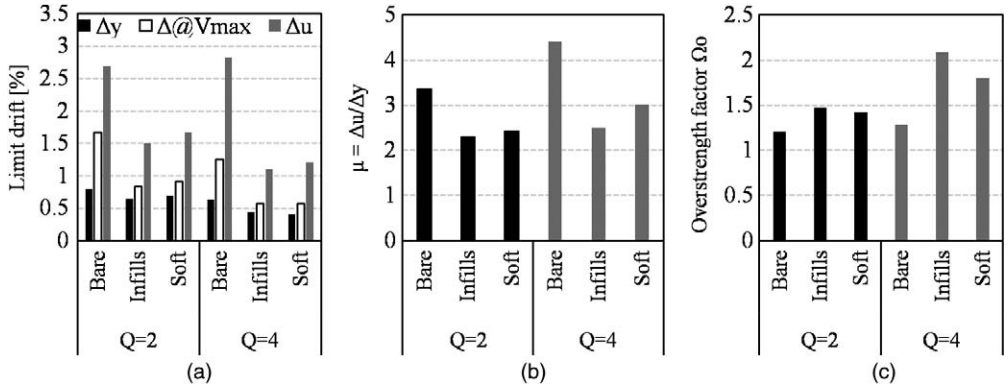

Figure 13. (a) Limit states of the roof drifts, (b) ductility capacity, and (c) overstrength factor for the evaluated six conditions.

Figure 14 depicts the deformed shape of the building when the ultimate state is reached. Plastic hinge demand at the beam and column ends is depicted with colored circles indicating the curvature ductility demand (i.e., ϕ/ϕ_y). For buildings with $Q = 2$, an upper-story mechanism is formed between the second and the fifth floor (i.e., the columns yield at the bottom of the second story and at the top of the fourth story, while all beams yield in the third and fourth floor). For buildings with $Q = 4$, the mechanism comprises 3–4 stories from the base. This is confirmed by posterior dynamic analyses. It is hypothesized that the lack of a strong column/weak beam provision in the building code prevented a uniform distribution of yielding at the beam ends along the height of the structures, hence inhibiting a more ductile behavior.

NONLINEAR DYNAMIC ANALYSES

For the nonlinear dynamic analyses, mass and stiffness-proportional Rayleigh damping was included to simulate the energy dissipation characteristics of the building not represented by the nonlinear behavior of the framing elements. The coefficients in the Rayleigh damping formulation were established to achieve damping ratio of $\zeta = 2.5\%$ at periods corresponding to the first and third vibrational periods of the model.

Two definitions of structural periods are considered from the inelastic models (see Table 4): (1) the initial period (T_0) of vibration after applying the gravitational loading, which accounts for some service-loading cracking; and (2) a cracked period of vibration based on the static nonlinear response. The initial periods of the structures varied from 0.80 to 1.71 s, being 26% shorter, on average, for the structures with $Q = 2$ compared with those with $Q = 4$. The addition of the infills shortens the structural period by approximately 30%. The idealized pushover curves in Figure 12b were scaled to an ISDOF backbone following the procedure by Chopra and Goel (2002). By doing so, the initial slope of the equivalent ISDOF curve is proportional to the square of the cracked circular frequency of vibration (ω_{cr}^2), and the corresponding cracked period (T_{cr}) is consistent with a secant-to-yielding stiffness. For the bare frames, the ratio T_{cr}/T_0 is 1.53 and 1.31 for $Q = 2$ and

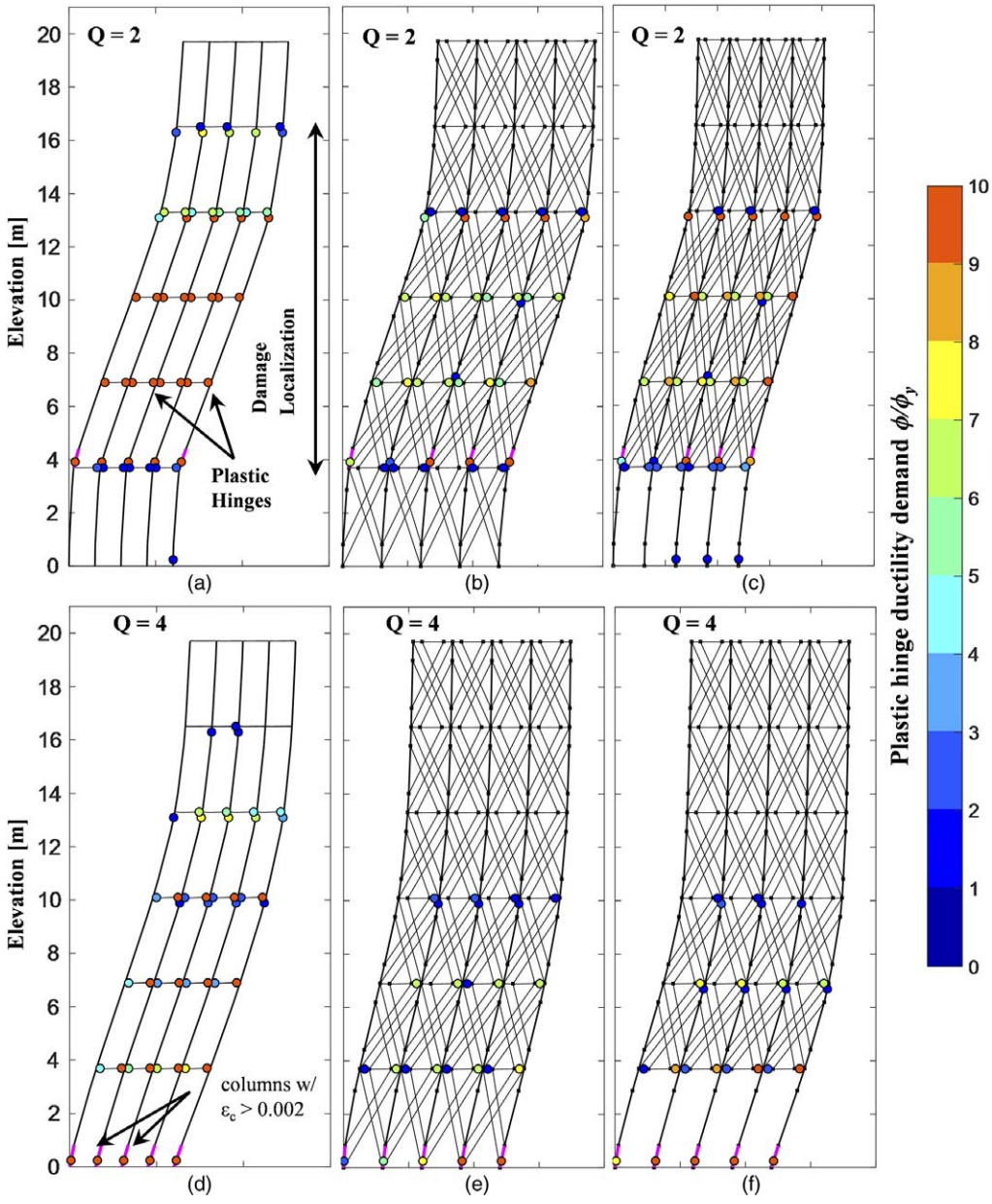

Figure 14. Deformed shape of the building and projection of plastic hinges (colored filled circles) at ultimate state for (a) $Q = 2$ bare frame, (b) $Q = 2$ fully infilled frame, (c) $Q = 2$ frame with soft story, (d) $Q = 4$ bare frame, (e) $Q = 4$ fully infilled frame, and (f) $Q = 4$ frame with soft story.

Table 4. Periods of vibration of the inelastic models

	$Q = 2$ initial period, T_0 (s)	$Q = 2$ cracked period, T_{cr} (s)	$Q = 4$ initial period, T_0 (s)	$Q = 4$ cracked period, T_{cr} (s)
Bare RC frame	1.20	1.84	1.71	2.24
Fully infilled RC frame	0.80	1.36	1.03	1.29
Partially infilled RC frame	0.86	1.46	1.16	1.42

$Q = 4$, respectively. For the infilled structures, this ratio becomes, on average, 1.70 and 1.24 for $Q = 2$ and $Q = 4$, respectively.

The inelastic models were analyzed dynamically with four pairs of two horizontal-component accelerograms input as uniform excitation at the base. Selected ground motions were recorded at the Mexico City stations closer to the structures visited and investigated by the reconnaissance team, namely SCT2, PCJR, LEAC, and TACY stations. The first three stations were chosen because of their proximity to the observed collapsed buildings. The TACY station is the only one on rock and is used here for calibration because no damage was reported around it. The structural response presented next corresponds to that induced by the horizontal component that produced the largest story drift ratio (SDR). Figure 15 shows the maximum SDR for the six models evaluated. It is apparent in the figure that the rock motions recorded at the TACY station induced the smallest responses among all evaluated ground motions. Although the LEAC records exhibited the largest elastic pseudo-acceleration coordinates among all records in Mexico City, this ground motion did not produce the largest SDR. In fact, except for the case of $Q = 2$ for frames with infills, responses under the LEAC input motion are third to those induced by the STC2 and PCJR motions. For $Q = 2$, maximum SDR for the bare frames is observed for the PCJR motion, while the SCT2 motion induced larger relative displacements for the frames with infills. For the weaker building, the PCJR record induced the largest SDR in all cases. This trend is consistent with the results presented in the following section, where the largest displacements are expected for systems subjected to the SCT2 and PCJR records, especially for $T \geq 1.0$ s.

It is worth noting that the structures with infills exhibited overall larger story drifts than those without them, especially those with $Q = 4$, where the drift demand is concentrated in the first story. Additionally, these structures have shorter period, which exacerbates their ductility demand. For the stronger building ($Q = 2$), the maximum computed SDR is close to 2.5% at the third floor, while for the $Q = 4$ buildings, this value is approximately 3% at the first story for structures with infills, and it is over 2% at the third floor for the bare frame. The dynamic analyses confirmed the high potential of damage localization in the first 2 stories for the weaker building with infills. For $Q = 4$, the SCT2 and the PCJR records induced localized damage in the first 2 stories even when infills were uniformly distributed over the entire building height. A question that arises is whether these structures are able to accommodate drift ratios as large as 2.5% in the middle third of the height or as large as 3% in the first story. Table 5 summarizes maximum SDR with location over the height of the structure and the ground motion that produced it.

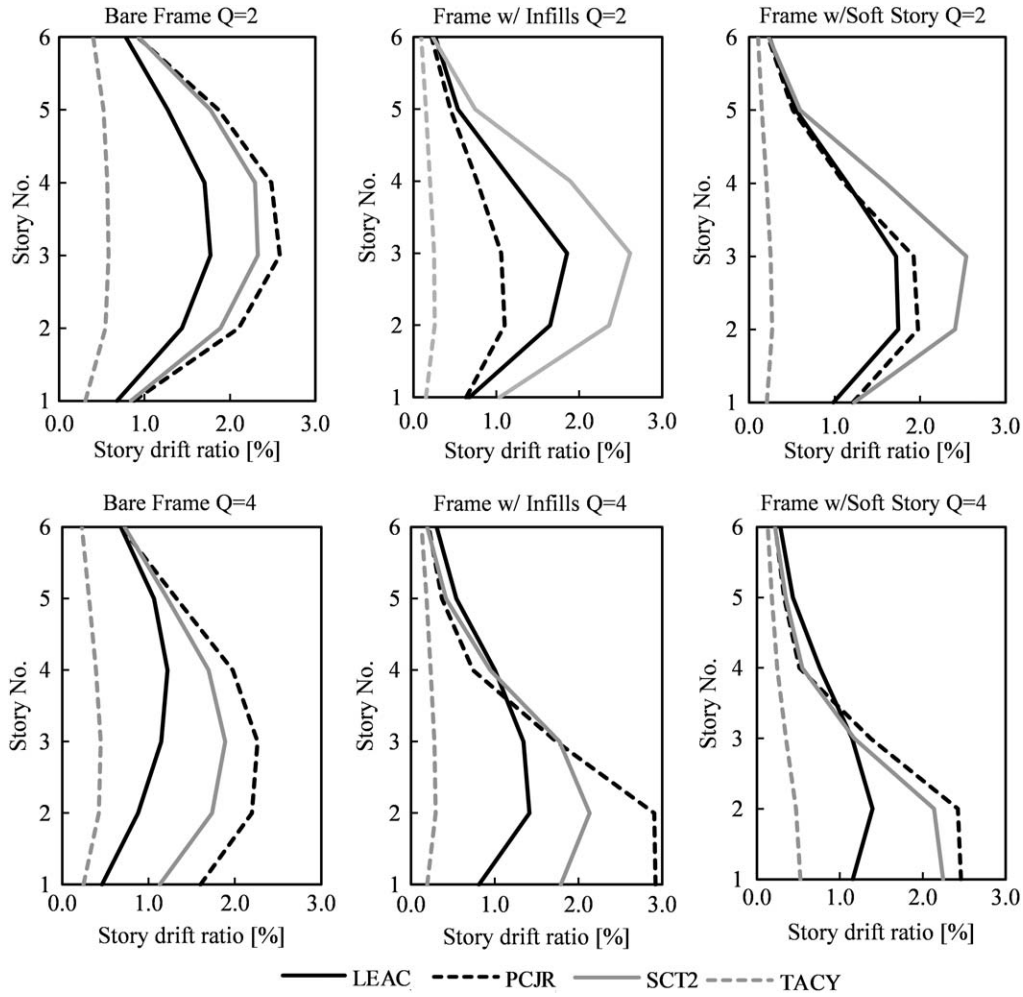

Figure 15. Maximum story drifts for $Q = 2$ and 4 because of LEAC, PCJR, SCT2, and TACY ground motion records.

Table 5. Maximum computed story drift ratio

	$Q = 2$			$Q = 4$		
	Bare	Fully infilled	Soft story	Bare	Fully infilled	Soft story
SDRmax	2.6%	2.6%	2.5%	2.3%	2.9%	2.5%
Story	3	3	3	3	1	1
Ground motion	PCJR	STC2	STC2	PCJR	PCJR	PCJR

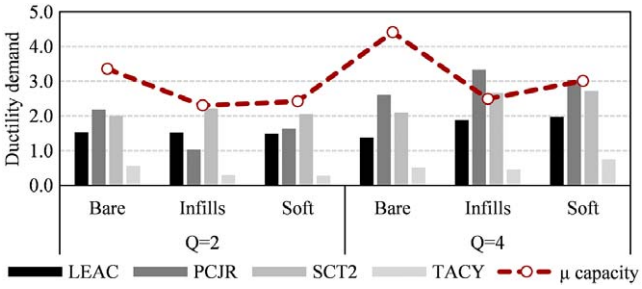

Figure 16. Ductility demand for $Q = 2$ and 4.

The maximum roof displacement demand from the dynamic analyses is normalized by the roof yield displacement from the pushover analyses to estimate the ductility demand. Figure 16 compares roof ductility capacities with their associated demands from the four different ground motion records used for theses dynamic analyses. While ductility demand for bare frames is lower than their capacity according to these results, ductility capacity of infilled frames is practically reached for the buildings designed with $Q = 2$ and exceeded for those designed with $Q = 4$.

As mentioned previously, though infill walls increase the strength of the lateral force–resisting system, they limit the deformation capacity. This is mainly due to the limited ductility and strength of masonry, which is considerably lower than those of the RC structural members. This implies that for low SDRs (e.g., SDR < 1%), the capacity of infills may be exceeded and severe damage induced. To assess the damage level in infills, a damage index (*DI*) is defined as the ratio between the deformation demand ε_{max} of the struts representing the infills and their deformation at peak stress, ε_{mo}, previously defined (Figure 11c). Values of *DI* lower or equal to 1.0 indicate that the struts were not excited beyond the elastic range, while greater values indicate that permanent deformation of theses struts are expected. Figure 17 presents the maximum average *DI* per story and ground motion for the previously defined models of the infilled frames. Results indicate that SCT2 induced more damage in infills compared with other records for structures designed with $Q = 2$, while PCJR and SCT2 induce the most significant damage for structures with $Q = 4$. This trend is in accordance with results presented in Figure 16, where these motions demanded more ductility capacity for the models. Damage is more significant in the second and third stories for $Q = 2$, though it tends to distribute over the height. On the other hand, for $Q = 4$, damage is basically concentrated in the first and second stories. Values of *DI* are the greatest for $Q = 4$, with infills distributed over the entire height when the system is subjected to PCJR and SCT2 motions. While the average *DI* only varies marginally, for these two motions, between the infilled and soft story structure with $Q = 2$, it does reduce to approximately one-half for the structure with $Q = 4$, confirming that the soft story acts as a fuse for the weaker system, and the upper stories displace as a rigid block.

ISDOF SYSTEM RESPONSE

Simplification of complex multi-degree-of-freedom (MDOF) structural systems to ISDOF systems has been proven to be an efficient approach to perform seismic response assessment of buildings with different dynamic characteristics (Takeda et al. 1970,

Maximum Struts Damage Index *DI*

Q = 2 Frame with Infills

Story	LEAC	PCJR	SCT2	TACY
6	0.5	0.4	0.4	0.2
5	0.9	0.8	0.9	0.3
4	1.9	1.7	1.9	0.4
3	3.7	3.2	4.3	0.5
2	3.6	3.4	5.2	0.5
1	1.5	1.8	1.9	0.4
AVG	2.0	1.9	2.4	0.4

Q = 2 Frame with soft story

Story	LEAC	PCJR	SCT2	TACY
6	0.6	0.4	0.4	0.2
5	1.1	0.9	1.0	0.3
4	2.2	2.0	2.8	0.4
3	3.3	3.5	4.6	0.5
2	3.4	3.6	4.4	0.5
1	-	-	-	-
AVG	2.1	2.1	2.6	0.4

Q = 4 Frame with Infills

Story	LEAC	PCJR	SCT2	TACY
6	0.4	0.5	0.3	0.2
5	1.1	0.9	0.7	0.3
4	2.0	1.6	1.7	0.4
3	2.4	3.1	3.2	0.5
2	2.0	5.3	3.9	0.5
1	1.2	6.2	3.7	0.4
AVG	1.5	2.9	2.3	0.4

Q = 4 Frame with soft story

Story	LEAC	PCJR	SCT2	TACY
6	0.5	0.4	0.3	0.2
5	0.9	0.5	0.5	0.3
4	1.3	1.0	0.9	0.4
3	2.0	1.9	1.7	0.5
2	2.2	2.6	3.0	0.8
1	-	-	-	-
AVG	1.4	1.4	1.3	0.5

Figure 17. Infills damage index *DI* for $Q = 2$ and 4 because of LEAC, PCJR, SCT2, and TACY ground motion records.

Saiidi and Sozen 1981, Gulkan and Sozen 1999, Ruiz-García and Miranda 2003). An ISDOF model is implemented next to extrapolate the results of the 6-story infilled frames of the previous section (i.e., those in Figures 9c, 14b and 14e) to other ranges of plausible periods. This is one step further to provide a plausible explanation of the damage observed on buildings of certain height in Mexico City and to provide contrast to the discussion presented above regarding elastic spectral demand.

The results presented in this section were obtained using OpenSees (McKenna et al. 2000). The uniaxial Hysteretic Material model developed by Scott and Filippou (2016) was implemented for this purpose. The ISDOF model implemented has a multilinear backbone (ML-model; Figure 10a) with hysteretic response similar to the Modified Clough model used by Ruiz-García and Miranda (2006) to simulate stiffness degradation during reloading but calibrated to replicate the nonlinear dynamic response of the case study models described before (Figure 10b). As shown in Figure 10a, for small displacements, the system is elastic with initial stiffness k_o up to a yield deformation u_y, where the system becomes plastic at load C_y, which refers to the yield strength expressed as a fraction of gravity. The model considers a post-yielding hardening defined by parameter β. The ultimate displacement is $D_u = \mu_c u_y$, where the ductility capacity ratio (μ_c) is specified to define the span of the strain hardening portion. For displacements larger than D_u, the strength degradation is specified with the parameters $D_x = \gamma u_y$ and ρ; where the ductility-like parameter γ specifies the span of the

softening portion up to achieving the residual capacity ρC_y. Values of β, μ_c, γ, and ρ are calibrated to follow the backbone in Figure 12b, which is previously scaled to an ISDOF backbone following the procedure by Chopra and Goel (2002).

Equations 2–5 define, respectively, the initial stiffness (k_0), the ultimate strength (C_{max}), the yield strength (C_y), and the yield displacement (u_y) of the ISDOF system. Variable k_0 is defined in terms of the cracked period in Table 4. Strength C_{max} is a function of the design spectral acceleration (S_a), the overstrength factor Ω, and the inverse of the effective modal mass ratio for the first mode M/M_1^*:

$$k_0 = \frac{1}{\left(\frac{T_{cr}}{2\pi}\right)^2} \tag{2}$$

$$C_{max} = S_a \Omega \frac{M}{M_1^*} \tag{3}$$

$$C_y = \frac{C_{max}}{1 + \beta(\mu_c - 1)} \tag{4}$$

$$u_y = C_y \left(\frac{T_{cr}}{2\pi}\right)^2 \tag{5}$$

Figure 10c shows the 1976 elastic ($Q = 1$) and reduced design spectra for Q values of 2 and 4. These spectral coordinates define the S_a values in Equation 3 to represent the strength of older-type of framing systems. Following the results in Figure 12b, factor Ω was selected as 1.80 for the infilled frames, which closely matched the mean overstrength for the $Q = 2$ and $Q = 4$ structures. Amplification of $S_a\Omega$ by M/M_1^* is necessary to match the strength of the MDOF system. This ratio is set to 1/0.80, which closely matches the estimates for all structural models. In addition to the energy dissipation provided by the hysteretic response, a 2.5% viscous damping ratio was selected for the model, which is the same as in the MDOF models.

For the ISDOF models evaluated herein, the ductility demand is the ratio between the maximum displacement experienced under any given ground motion (u_m) and the yield displacement, u_y (e.g., $\mu = u_m/u_y$). Figure 18 shows the ductility demand of the ISDOF systems representative of the infilled frame systems designed with $Q = 2$ and $Q = 4$ under the motions recorded in Mexico City. The horizontal axis in these figures is representative of the cracked period of the structures as described before. Ductility capacity of the older nonductile structures retrieved from MDOF models is highlighted using a dotted horizontal line. In order to compare ISDOF and MDOF results, predicted ductility demand for the case study buildings obtained from MDOF models is also depicted with squared and triangular markers. It is observed that the ISDOF model predicts well the ductility demand of the MDOF and hence validates the simplified modeling approach.

Figure 18 confirms that the TACY and CUP5 rock motions induced little to nonplastic demand on the infilled structures of any strength, while the ductility demand induced by the PISU and CCCL motions did not surpass the expected capacity of the buildings. These conclusions are consistent with the reduced or lack of structural damage observed around these

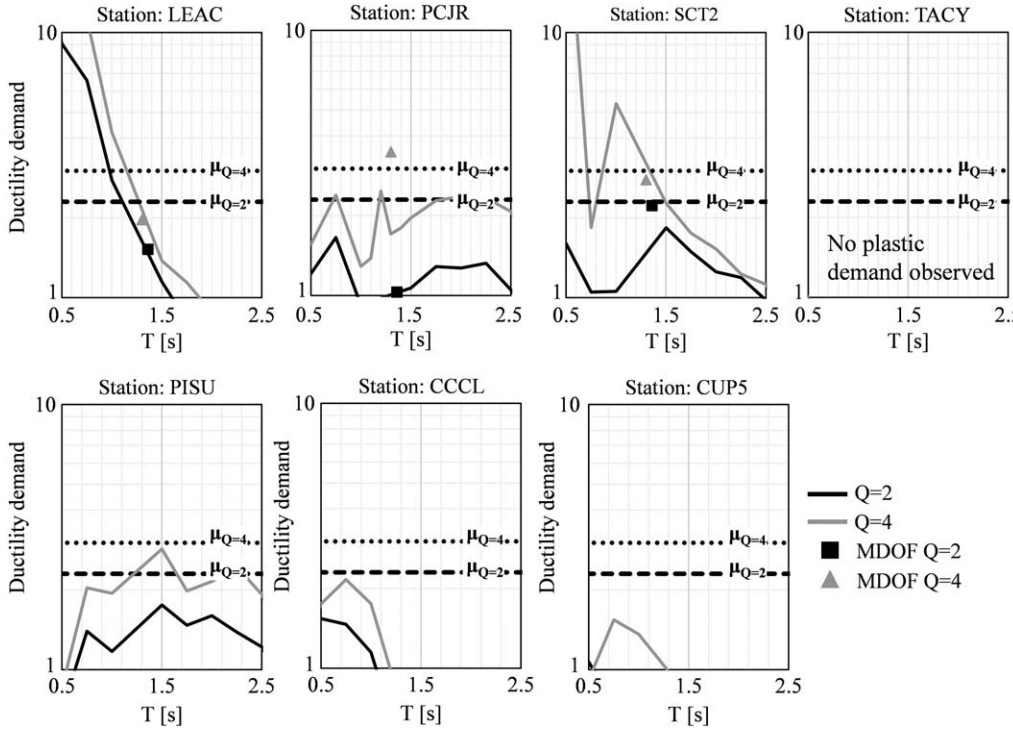

Figure 18. Ductility demand spectra for bare frames and infilled frames under LEAC, PCJR, SCT2, TACY, PISU, CCCL, and CUP5 motion

four stations. On the other hand, the demand on the LEAC and SCT2 stations show that the ductility capacity for weaker structures with $Q = 4$ may have been surpassed in the period range of the structures visited. It is noted that that the ductility demand for the LEAC station is above the capacity for either structural strength in the period range $0.50 \leq T \leq 1.15$ s, although it reduces at a constant rate for longer periods. Collapses of buildings shorter than 4 stories were observed close to this station (see Figure 1b). A similar situation occurs for the weaker structures under the SCT2 motion, where the ductility demand is beyond the capacity for $T \leq 1.35$ s. Considering $C_u T_a$, a lower bound of secant-to-yielding stiffness-based periods, this range of periods previously mentioned can be considered as representative of infilled frame buildings with 2 to 8 stories. The height of collapsed buildings around the SCT2 station varied between 3 and 6 stories. Lastly, the PCJR motion induced the largest demand on structures with $Q = 4$ with $T \geq 1.6$ s but did not necessarily surpass the expected capacity. Nevertheless, Figure 1b shows that the height of buildings that collapsed near this station ranged from 3 to 7 stories.

CONCLUDING REMARKS

One week after a Mw 7.1 earthquake struck the central region of Mexico on 19 September 2017, a post-earthquake reconnaissance mission was organized between the PEER and the

CEER to assess the response of structural and nonstructural components of over 60 buildings in Mexico City where the damage was concentrated. Field observations, statistical analysis of damage, and numerical experiments helped explain the extent of damage observed in mid-rise RC frame buildings with and without masonry infill walls. These mid-rise buildings are an archetypical structural system in Latin American Countries and worldwide. A significant number of currently functional similar buildings in Mexico were designed following older code requirements known to be insufficient to ensure acceptable performance under seismic loadings, as demonstrated in the 1985 and/or the 2017 Mexico earthquakes.

Comparison of the recoded ground motions with the global BCHydro model demonstrated that for structural periods between 0.5 and 1.0 s, the recorded ground motions in soil sites within Mexico City were not particularly rare. Although, for larger structural periods up to 2.0 s, their intensity was larger than the median intensity of global earthquakes of the same magnitude recorded at similar distances. In fact, ground motions recorded in the stations next to the observed collapsed were up to 5-times larger than the median global ground motion, which is associated with basin site effects.

Results from the SDOF and MDOF systems modeled in this study agreed in predicting high ductility demands for mid-rise buildings with cracked periods shorter than 1.5 s, approximately. Addition of non-isolated masonry infills during the construction of RC frames, which were originally analyzed and designed to be bare systems, significantly impact their ductility capacity. Results also confirmed the high potential of damage localization in the first 2 stories for pre-1985 flexible nonductile structures with infills. Furthermore, the masonry-frame interaction increased the potential for a soft-story mechanism formation. Numerical results also indicated that the accelerograms recorded in SCT2 and PCJR stations located in Mexico City induced the largest structural and nonstructural demand on mid-rise RC frame buildings with masonry infill walls. This is consistent with the distribution of damage identified in the field and reported by the reconnaissance teams.

In general, the ISDOF results agree with in-situ observations. The stations with the highest number of nearby collapses were LEAC, PCJR, and SCT2, which is consistent with the numerical simulations showing that the ductility capacity of mid-rise masonry-infilled RC-framed buildings was exceeded, specifically, in those designed with the larger seismic force reduction factor $Q = 4$.

ACKNOWLEDGMENTS

Funding for the CEER team was provided by Universidad del Norte, Universidad Militar Nueva Granada, Escuela de Ingeniería de Antioquia, Universidad de Medellín, and Asociación Colombiana de Ingeniería Sísmica (AIS). The PEER partners were funded by the Pacific Earthquake Engineering Research Center at University of California Berkeley. Special thanks to Sergio Alcocer and Mario Rodriguez from UNAM and for providing important logistical support to the reconnaissance team.

REFERENCES

Abrahamson, N. A., Gregor, N., and Addo, K., 2016. BCHydro ground motion prediction equations for subduction earthquakes, *Earthquake Spectra* **32**, 23–44.

Ancheta, T. D., Darragh, R. B., Stewart, J. P., Seyhan, E., Silva, W. J., Chiou, B. S. -J., Wooddell, K. E., Graves, R. W., Kottke, A. R., Boore, D. M., Kishida, T., and Donahue, J. L., 2014. NGA-West2 Database, *Earthquake Spectra* **30**, 989–1005.

Arteta, C. A., 2015. Seismic Response Assessment of Thin Boundary Elements of Special Concrete Shear Walls, Ph.D Thesis, University of California, Berkeley, CA.

American Society of Civil Engineers (ASCE), 2016. *Minimum Design Loads for Buildings and Other Structures, ASCE/SEI 7-16*, Reston, VA.

Bommer, J. J., and Akkar, S., 2012. Consistent source-to-site distance metrics in ground-motion prediction equations and seismic source models for PSHA, *Earthquake Spectra* **28**, 1–15.

Carrillo, J., Hernández-Barrios, H., and Rubiano-Fonseca, A., 2014. Analysis of the earthquake-resistant design approach for buildings in Mexico, *Ingeniería, Investigación y Tecnología* **15**, 151–162.

Coleman, J., and Spacone, E., 2001. Localization issues in force-based frame elements, *Journal of Structural Engineering* **127**, 1257–1265.

Crisafulli, F. J., 1997. Seismic Behaviour of Reinforced Concrete Structures with Masonry Infills, Ph.D Thesis, University of Canterbury, Christchurch.

Crisafulli, F. J., Carr, A. J., and Park, R., 2005. Experimental response of framed masonry structures designed with new reinforcing details, *Bulletin of the New Zealand Society for Earthquake Engineering* **38**, 19–32.

Chávez-García, F. J., and Bard, P. -Y., 1994. Site effects in Mexico City eight years after the September 1985 Michoacan earthquakes, *Soil Dynamics and Earthquake Engineering* **13**, 229–247.

Chopra, A. K., and Goel, R. K., 2002. A modal pushover analysis procedure for estimating seismic demands for buildings, *Earthquake Engineering & Structural Dynamics* **31**, 561–582.

Chrysostomou, C. Z., Gergely, P., and Abel, J. F., 2002. A six-strut model for nonlinear dynamic analysis of steel infilled frames, *International Journal of Structural Stability and Dynamics* **2**, 335–353.

European Seismological Commission (ESC), 1998. *European Macroseismic Scale 1998*, Luxembourg.

Federal Emergency Management Agency (FEMA), 2009. *Quantification of Building Seismic Performance Factors, Tech. Rep. FEMA-P695*, Washington, DC.

Federal Emergency Management Agency (FEMA), 2015. *NEHRP Recommended Seismic Provisions for New Buildings and Other Structures, Tech. Rep. FEMA-P1050-1*, Washington, DC.

Garcia, D., Singh, S., Herráiz, M., Ordaz, M. G., and Pacheco, J., 2005. Inslab earthquakes of Central Mexico: Peak ground-motion parameters and response spectra, *Bulletin of the Seismological Society of America*, **95**, 2272–2282.

Global Earthquake Model (GEM), 2014. *Report on the SARA Exposure and Vulnerability Workshop in Medellin Colombia, GEM Foundation*, Pavia, Italy.

Global Earthquake Model (GEM), 2016. *How Exposed is South America to Earthquakes?*, Pavia, Italy.

Gulkan, P., and Sozen, M. A., 1999. Procedure for determining seismic vulnerability of building structures, *Structural Journal* **96**.

Han-Seon, L., and Sung-Woo, W., 2002. Effect of masonry infills on seismic performance of a 3-storey R/C frame with non-seismic detailing, *Earthquake Engineering & Structural Dynamics* **31**, 353–378.

Hashemi, A., and Mosalam, K. M., 2006. Shake-table experiment on reinforced concrete structure containing masonry infill wall, *Earthquake Engineering & Structural Dynamics* **35**, 1827–1852.

Jansen, D. C., and Shah, S. P., 1997. Effect of length on compressive strain softening of concrete, *Journal of Engineering Mechanics* **123**, 25–35.

Kramer, S. L., 1996. *Geotechnical Earthquake Engineering*, Pearson, Upper Saddle River, NJ.

Mayoral, J. M., Hutchinson, T. C., and Franke, K. W., 2017. *Geotechnical Engineering Reconnaissance of the 19 September 2017 Mw 7.1 Puebla-Mexico City Earthquake, Version 2.0, Tech. Rep. GEER-055A*, Geotechnical Extreme Events Reconnaissance Association.

Mazzoni, S., McKenna, F., and Fenves, G. L., 2007. Steel02 & hysteretic – material behavior, in *OpenSees Comparison of Modelling Tools*, Pacific Earthquake Engineering Research Center, Berkeley, CA.

McKenna, F., Fenves, G. L., Scott, M. H., and Jeremic, B., 2000. *Open System for Earthquake Engineering Simulation (OpenSees), Version 2.4.3.*, software, http://opensees.berkeley.edu/

Mehrabi, A. B., Benson Shing, P., Schuller, M. P., and Noland, J. L., 1996. Experimental evaluation of masonry-infilled RC frames, *Journal of Structural Engineering* **122**, 228–237.

Meli, R., 1994. Structural design of masonry buildings: the Mexican practice, *American Concrete Institute, ACI Special Publication* **147**, 239–262.

Mexican School of Civil Engineers (CICM), 2017. *Resumen preliminar de daños de los inmuebles inspeccionados por las brigadas del CICM del Sismo del 19/09/2017*, Mexico City, Mexico.

Mosalam, K. M., and Günay, S., 2015. Progressive collapse analysis of reinforced concrete frames with unreinforced masonry infill walls considering in-plane/out-of-plane interaction, *Earthquake Spectra* **31**, 921–943.

Muriá, D., and González, R., 1995. Dynamic properties of building in Mexico City, *Ingeniería Sísmica* **351**, 24–45.

National Autonomous University of Mexico (UNAM), 2017. *Parámetros del Movimiento del Suelo Sismo de Puebla-Morelos (Mw 7.1) 19 de septiembre de 2017*, Mexico City, Mexico.

NTC-C, 1976. *Normas Tecnicas Complementarias para Diseño y Construcción de Estructuras de Concreto, Gaceta Oficial del Distrito Federal*, Mexico City, Mexico.

NTC-S, 1976. *Normas Tecnicas Complementarias para Diseño por Sismo, Gaceta Oficial del Distrito Federal*, Mexico City, Mexico.

NTC-S, 2004. *Normas Tecnicas Complementarias para Diseño por Sismo, Gaceta Oficial del Distrito Federal*, Mexico City, Mexico.

ONNCE, 2012. *Industria de la Construcción - Mampostería - Bloques, Tabiques o Ladrillos y Tabicones para Uso Estructural – Especificaciones y Métodos de Ensayo, NMX-C-404-ONNCCE-2012*, Mexico City, Mexico.

Ordaz, M., Miranda, E., and Avilés, J., 2003. Propuesta de espectros de diseño por sismo para el DF, *Revista Internacional de Ingeniería de Estructuras* **8**, 189–207.

Reinoso, E., Jaimes, M. A., and Torres, M. A., 2016. Evaluation of building code compliance in Mexico City: Mid-rise dwellings AU – Reinoso, Eduardo, *Building Research & Information* **44**, 202–213.

Ruiz-García, J., and Miranda, E., 2003. Inelastic displacement ratios for evaluation of existing structures, *Earthquake Engineering & Structural Dynamics* **32**, 1237–1258.

Ruiz-García, J., and Miranda, E., 2006. Inelastic displacement ratios for evaluation of structures built on soft soil sites, *Earthquake Engineering & Structural Dynamics* **35**, 679–694.

Sahakian, V. J., Melgar, D., Quintanar, L., Ramírez-Guzmán, L., Pérez-Campos, X., and Baltay, A., 2018. Ground motions from the 7 and 19 September 2017 Tehuantepec and Puebla-Morelos, Mexico, Earthquakes, *Bulletin of the Seismological Society of America* **108**, 3300–3312.

Saiidi, M., and Sozen, M. A., 1981. Simple nonlinear seismic analysis of R/C structures, *Journal of the Structural Division* **107**, 937–953.

Scott, M., and Filippou, F. C., 2016. Hysteretic material, available at http://opensees.berkeley.edu/wiki/index.php/Hysteretic_Material (last accessed 16 November 2018).

Spacone, E., Filippou, F. C., and Taucer, F. F., 1996. Fibre beam-column model for non-linear analysis of R/C frame: Part I. Formulation, *Earthquake Engineering and Structural Dynamics* **25**, 711–725.

Takeda, T., Sozen, M. A., and Nielsen, N. N., 1970. Reinforced concrete response to simulated earthquakes, *Journal of the Structural Division* **96**, 2557–2573.

U.S. Geological Survey (USGS), 2017. Updated finite fault results for the Sep 19, 2017 Mw 7.1 earthquake (version 2), available at https://earthquake.usgs.gov/archive/product/finite-fault/us2000ar20/us/1506135689560/2000ar20.html (last accessed 12 April 2018).

Wittmann, F., Rokugo, K., Brühwiler, E., Mihashi, H., and Simonin, P., 1988. Fracture energy and strain softening of concrete as determined by means of compact tension specimens, *Materials and Structures* **21**, 21–32.

(Received 12 June 2018; Accepted 3 May 2019)